# Cultured Podocytes Establish a Size-Selective Barrier Regulated by Specific Signaling Pathways and Demonstrate Synchronized Barrier Assembly in a Calcium Switch Model of Junction Formation

Jennifer L. Hunt, Martin R. Pollak, and Bradley M. Denker
*Renal Division, Department of Medicine, Brigham and Women's Hospital, Boston, Massachusetts*

**Podocytes form unique cell–cell junctions (slit diaphragms) that are central to glomerular selectivity, although regulation and mechanisms of slit diaphragm assembly are poorly understood. With the use of cultured podocytes, a paracellular permeability flux assay was established to characterize properties of the size-selective barrier. Paracellular flux of differentiated podocytes was measured using anionic fluorescent dextrans of 3, 10, 40, and 70 kD. Podocytes form a highly selective barrier with a 160-fold difference in flux from the 3-kD dextran (11 pmol/min) to the 70-kD dextran (0.06 pmol/min). Barrier development was dependent on podocyte differentiation and not affected by dextran charge. Puromycin, a known podocyte toxin, increased flux 250% in a dose-dependent manner without affecting cell viability. Screening with modulators of specific signaling pathways identified reversible increases in flux with Src tyrosine and Rho kinase inhibition. The calcium switch model of epithelial junction assembly was modified to determine whether podocytes regulate barrier assembly. When cultured in low calcium for 90 min, flux increased by 300% and consistently returned to baseline 24 to 48 h after switching to normal calcium. Similar to classical epithelial junctions, barrier recovery occurred in the presence of cyclohexamide, an inhibitor of protein synthesis. During the calcium switch, there were reversible changes in localization and detergent solubility of the slit diaphragm protein ZO-1 and α-actinin-4, whereas nephrin and podocin solubility were unchanged. Taken together, these findings demonstrate that cultured podocytes develop a selective size barrier that is regulated by specific signaling pathways, and similar to classical epithelial junctions, podocytes demonstrate synchronized assembly of the barrier.**
*J Am Soc Nephrol* 16: 1593–1602, 2005. doi: 10.1681/ASN.2004080679

The glomerulus is a complex and highly selective barrier that is crucial to maintaining normal body homeostasis. It is frequently a site of injury in both renal-specific diseases and common systemic disorders that affect the kidney. Injury to the filtration barrier is typically manifested with the leakage of plasma proteins (proteinuria), which is often the first indication of renal disease. The properties of this intricate barrier and the disturbances that lead to proteinuria are not fully understood. Recent evidence suggests that proteinuria is an *independent* risk factor for progressive decline in renal function and development of ESRD (1). Therefore, understanding the mechanisms that are responsible for glomerular selectivity are essential for identifying therapeutic strategies to protect and/or restore the barrier in pathophysiologic conditions.

Forming a unique fenestrated microcirculation, the glomerulus is uniquely specialized for ultrafiltration. The glomerular capillary wall is composed of three major components: a fenestrated endothelium, a 300-nm-thick glomerular basement membrane (GBM), and visceral epithelial cells (podocytes). Transglomerular movement of proteins across the capillary wall is limited by factors such as size, shape, and charge (2,3). However, experimentally defining the contribution of endothelial cells, GBM, and podocytes to glomerular selectivity *in vivo* is a nearly impossible task (4–6). Podocytes form an extensive network of interdigitated foot processes; the junctions between these processes are termed slit diaphragms and are in many ways similar to epithelial adherens junctions (7). The slit diaphragm is composed of membrane and cytoskeletal proteins in addition to signaling molecules. Some of the recently discovered proteins are unique to podocytes (*e.g.*, nephrin, podocin, neph1–3 [8–10]), whereas some, such as CD2AP and α-actinin-4, were initially identified in other cell types and subsequently discovered to have important roles in the podocyte (11,12). Finally, podocytes express well-characterized tight and adherens junction proteins, including ZO-1, cadherins, catenins, and MAGI-1 (7,13,14).

The development of a cultured podocyte cell line (15) has led to extensive new insights into the biology of these unique epithelial cells (reviewed in reference 16). However, a functional assay that permits dynamic studies of barrier function has been lacking. We asked whether cultured podocytes demonstrate a size-selective barrier and, if so, whether this could be used for signaling studies. Furthermore, an important question could now be addressed: Can podocytes reestablish barrier function from existing protein complexes in a manner analo-

*Received August 17, 2004. Accepted March 1, 2005.*

*Published online ahead of print. Publication date available at www.jasn.org.*

**Address correspondence to:** Dr. Bradley M. Denker, Harvard Institutes of Medicine, 77 Avenue Louis Pasteur, Boston, MA 02115. Phone: 617-525-5809; Fax: 617-525-5830; E-mail: bdenker@rics.bwh.harvard.edu


ISSN: 1046-6673/1606-1593

gous to classical epithelial cell junctions? We used a range of fluorescent dextran molecules to assess paracellular flux across podocyte monolayers. We find that barrier function of cultured podocytes reproduces several properties of *in vivo* glomerular selectivity, and size selectivity can be modulated by inhibition of specific signaling pathways. In addition, podocytes can reassemble the barrier in a calcium-dependent model of junction assembly.

## Materials and Methods

### *Cell Culture*

The generation of this immortalized mouse podocyte cell line was described previously (17). Podocytes were maintained in RPMI 1640 medium (Cellgro, Herndon, VA) and supplemented with 10% FCS and 10 U/ml mouse recombinant γ-IFN (Sigma, St. Louis, MO) for permissive conditions (33°C). Dishes were coated with type I collagen (BD Biosciences, Palo Alto, CA), and cells were plated at a density of $1 \times 10^5$ cells/cm$^2$. Differentiation was induced by switching to 37°C (nonpermissive conditions) and removing γ-IFN from the culture media. Differentiation was considered complete after 14 d as previously established (17).

### *Permeable Support System*

Permeable supports (Transwell; Corning Life Sciences, Acton, MA) of 6.5-mm diameter with 0.4-μm pore size were used in the paracellular flux assay, and a 12-mm filter with 0.4-μm pore size was used for immunohistochemical staining. Podocytes were grown under permissive conditions and allowed to reach 90% confluence. Cells then were plated on filters at confluent density ($1 \times 10^5$ cells/ml). The monolayers were differentiated for 14 d with a medium change every 48 h before paracellular flux was assessed.

### *Paracellular Flux Assay*

FITC-tagged anionic dextrans or Texas Red–tagged neutral dextrans of 3, 10, 40, and 70 kD (Molecular Probes, Eugene, OR) were used for determining paracellular fluxes. Dextrans were applied to the apical chamber (0.25 mg/ml) after washing with PBS. One milliliter of Hanks buffered salt solution (HBSS; Sigma) was added to the bottom chamber, and 0.2 ml of dextran was added to the top. Monolayers were incubated at 37°C for 80 min with shaking. Twenty-five-microliter aliquots were taken from the bottom chambers at 20, 40, 60, and 80 min, and fluorescence was measured using a Cytofluor 4000 fluorometer (Applied Biosystems, Foster City, CA).

### *Flux Calculations*

Arbitrary fluorescence units were imported into GraphPad Prism (GraphPad, San Diego, CA) for analysis. Standard curves were performed with each experiment. Linear regression analysis of the standard curve data ($R^2 > 0.99$) was used to convert experimental data into dextran concentration (pmol/ml). Fluxes (slopes) were calculated from a linear regression analysis of arbitrary units over time using 3 to 12 replicates per data point per experiment. Slopes for each experimental condition had $R^2$ values >0.9. Monolayers with dead or dying cells, empty filters, and scratched filters failed to demonstrate linear flux, had $R^2$ <0.5, and were excluded. The SE was calculated from the pooled slopes for each data point. Monolayer integrity was confirmed using a 2000-kD FITC-dextran that showed no detectable flux over 80 min.

### *Cell Viability*

Trypan blue staining was used to quantify cell viability. Podocytes were differentiated, trypsinized, gently centrifuged, and resuspended in 5 ml of HBSS. An aliquot that contained 0.2% trypan blue was incubated at room temperature for 15 min, and blue cells were counted on a hemocytometer. The percentage of trypan blue–positive cells was averaged over five fields of 12 to 57 cells.

### *Calcium Switch*

Podocytes were grown on 6.5-mm Transwells, and flux was determined after low calcium (LC) exposure (18). Filters were washed with calcium- and magnesium-free (Ca/Mg-free) HBSS, and Ca/Mg-free HBSS was added to the bottom chamber. After 90 min, flux was determined (LC condition) as described above. Flux was measured at specific times after switching from LC to normal calcium (NC) medium.

### *Detergent Extractions*

Detergent-soluble and -insoluble fractions were prepared as based on the method of Singh *et al.* (19). Extractions were done at specific times using 0.5 ml of lysis buffer (10 mM HEPES [pH 7.2], 1% Triton X-100, 100 mM NaCl, and 1× protease inhibitor cocktail [Roche Diagnostics, Basel, Switzerland]). Cells were scraped in lysis buffer, incubated for 20 min at 4°C, and centrifuged at 10,000 × *g* for 5 min. The supernatant (S; soluble fraction) was collected, and the pellet was resuspended in solubilization buffer (10 mM HEPES [pH 7.2], 1% SDS, 100 mM NaCl, and protease inhibitor cocktail [Roche Diagnostics]). The cell suspension was sonicated on ice, incubated for 20 min at 4°C, and centrifuged at 10,000 × *g* for 20 min. The resulting supernatant was labeled R (resistant fraction). Equivalent volumes of each fraction were analyzed by SDS-PAGE and Western blotting with anti–ZO-1 (Zymed, San Francisco, CA), anti-nephrin (courtesy of Larry Holtzman), anti-podocin (Zymed), and anti–α-actinin-4 (20).

### *Immunofluorescent Microscopy*

Podocytes were cultured on 12-mm Transwell filters, and a calcium switch was performed. Filters at baseline, in LC, and at points during NC recovery were fixed with 4% paraformaldehyde and blocked/permeabilized with 5% BSA in 0.05% Triton X-100. FITC-conjugated phalloidin (Molecular Probes) was used to stain actin followed by staining with rabbit anti–ZO-1 for 1 h. After three washes in PBS, Texas-Red donkey anti-rabbit secondary antibody (Sigma) was added at 1:1600 for 1 h. Filters were washed with PBS and mounted on glass slides. Images were obtained using a Nikon Labophot-2 microscope with Spot digital camera and software (version 3.5.7; www.diaginc.com/SpotSoftware), and figures were assembled using Adobe Photoshop and Illustrator (San Jose, CA).

## Results

### *Cultured Podocytes Demonstrate a Size-Selective Barrier*

Fluxes of anionic dextrans of 3, 10, 40, or 70 kD were measured as described in the Material and Methods section. There was a 160-fold spread in absolute flux between the 3- and 70-kD dextrans (ranging from 11 pmol/min for the 3-kD dextran to 0.06 pmol/min for the 70-kD dextran; Figure 1A). Flux for 10- and 40-kD dextrans were in between these two extremes at 1.4 (40 kD) and 0.27 pmol/min (10 kD). Parallel experiments with several additional cell lines compared the selectivity range between 3- and 70-kD dextrans (Figure 1B). Podocytes demonstrated the greatest range of selectivity (160×), and human microvascular endothelial cells (HMEC) were also selective, although less than podocytes (18×). As expected for a tight monolayer, Madin-Darby canine kidney (MDCK) cells showed no measurable flux with 70 kD, and fibroblasts (3T3 cells) were relatively nonselective (8×). A blank filter was included in every analysis, and flux was typically >250 pmol/min (Figure 1A; note break in scale).

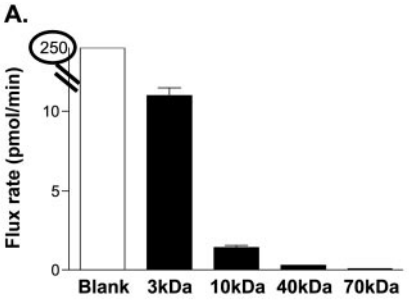


B.

| | Flux of 3kDa | Flux of 70kDa | Selectivity Range |
|---|---|---|---|
| Podocytes | 11.0 | 0.067 | 160x |
| MDCK | 0.033 | 0 | N/A |
| HMEC | 10.6 | 0.6 | 18x |
| 3T3 | 12.9 | 1.6 | 8x |

*Figure 1.* Cultured podocytes show size selectivity. (A) Paracellular flux of differentiated podocyte monolayers using FITC-dextrans (3, 10, 40, and 70 kD) was determined as described in the Materials and Methods section. Note the break in scale for flux of blank filter (□). (B) Absolute flux rates and selectivity range for podocytes, Madin-Darby canine kidney (MDCK) cells, human microvascular endothelial cells (HMEC), and 3T3 fibroblasts. Selectivity range was determined by 3-kD flux/70-kD flux. Results are the mean of 2 to 4 independent experiments ± SEM with $n = 6$ in each experiment.

To determine the effect of podocyte differentiation on barrier development, we determined flux at various times in culture under permissive conditions. There was a progressive tightening of the barrier over the 14-d differentiation period (Figure 2) for each of the fluorescence dextrans. The largest increase in barrier tightness was demonstrated with the 70-kD dextran, showing a nearly 10-fold decrease in flux (0.58 to 0.06 pmol/min). To control for cell number during differentiation, cells were plated at confluent density, trypsinized, and counted at each time point. There was no difference in the number of cells (6 to $8 \times 10^4$ cells/ml), verifying that progressive tightness was not a function of increased cell number.

Current modeling of the slit diaphragm in podocytes suggests that charge selectivity resides at the level of the basement membrane, not the podocyte (4,21). To determine the effect of charge on flux in this model, we used Texas Red–conjugated neutral dextrans in parallel with anionic FITC-dextrans (cationic dextrans are not available). Consistent with current models, we found no difference with neutral *versus* anionic dextrans on flux with each dextran (Figure 3). Transepithelial resistance was also measured in confluent podocyte monolayers and found to be $<10$ ohm/cm$^2$, a value similar to endothelial cells.

### *Puromycin Induces an Irreversible Increase in Paracellular Flux*

Puromycin (a known podocyte toxin) is frequently used as a model of glomerular injury. Puromycin treatment of cultured podocytes leads to reorganization of the actin cytoskeleton and slit diaphragm proteins (22,23). As shown in Figure 4A, puromycin exposure for 48 h at increasing concentrations from 5 to 30 $\mu$g/ml resulted in a dose-dependent increase in flux up to 200% of the control. Puromycin exposure for 48 h at 30 $\mu$g/ml was followed by incubation in puromycin-free medium for 24 and 48 h. There was no recovery of barrier function at either time point (Figure 4B). Trypan blue staining demonstrated no significant difference in positive cells with and without puromycin (6 *versus* 7%), indicating that toxicity from puromycin exposure is unlikely to account for these findings. Furthermore, a recent study found significant podocyte detachment only at higher puromycin concentrations for exposures of at least 48 h (24).

### *Modulation of Signaling Pathways Affects Paracellular Flux*

We tested a variety of signaling modulators on paracellular flux (Figures 5 and 6). Multiple lines of evidence indicate the

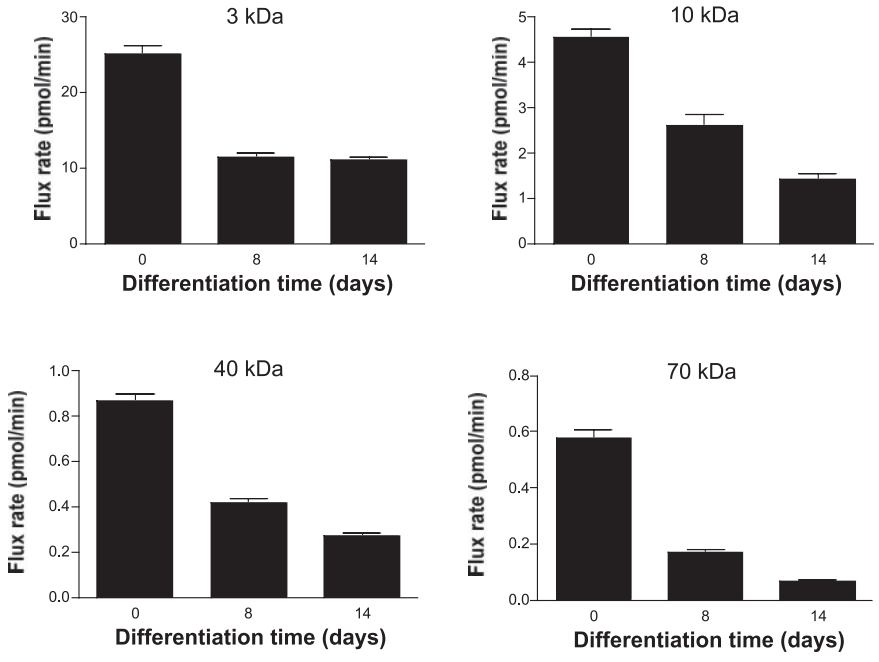


*Figure 2.* Tightening of barrier correlates with podocyte differentiation. Podocytes were grown for 14 total days, and filters were switched to nonpermissive conditions at various time points to obtain different stages of differentiation. Flux was measured as described in the Materials and Methods section. Results are the mean of two independent experiments ± SEM with $n = 6$ in each experiment. Differentiation under these conditions did not affect cell number as determined from trypsinized plates with 6 to $8 \times 10^4$ cells/cm$^2$ at each time point.

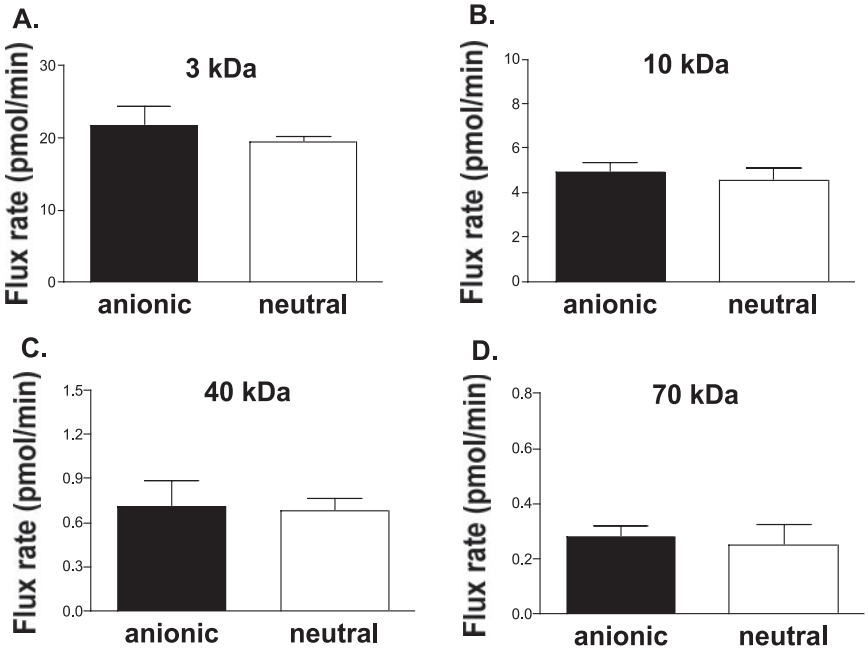


*Figure 3.* Paracellular flux of neutral dextran is similar to anionic dextran. Flux rates using anionic (■) and neutral (□) dextrans were compared: 3 kD (A), 10 kD (B), 40 kD (C), and 70 kD (D). Results are the mean of four independent experiments ± SEM with $n = 3$ in each experiment.

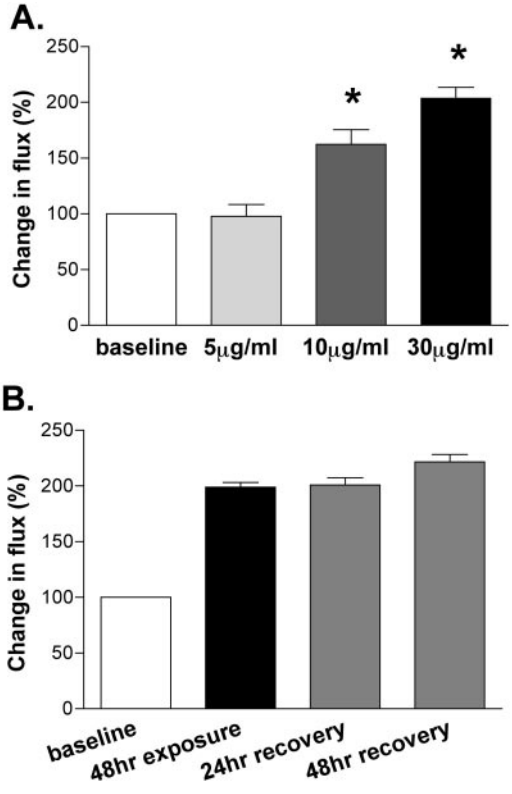


*Figure 4.* Puromycin irreversibly disrupts barrier. (A) Puromycin dose-response curve with 48 h of exposure to 5, 10, and 30 $\mu$g/ml. Flux rates are shown relative to baseline (no puromycin). *Statistically significant increase relative to baseline. (B) Puromycin (30 $\mu$g/ml) exposure for 48 h followed by recovery of 24 and 48 h. All data are with the 70-kD dextran and all fluxes are relative to baseline (□). Results are the mean of two independent experiments ± SEM with $n = 6$ in each experiment.

importance of Src tyrosine kinases in podocyte signaling (25). Treatment with the Src-specific inhibitor PP2 lead to a time-dependent increase in flux of 194% at 24 h and 252% at 48 h (Figure 5A). Genistein (a less specific tyrosine kinase inhibitor) showed a similar effect on flux at 48 h (data not shown). In cells that were exposed to PP2 for 48 h followed by removal, there was partial recovery of fluxes at 24 h, although no further recovery at 48 h. Trypan blue staining confirmed that toxicity was not likely to be responsible for the changes in flux (9% with PP2 *versus* 7%).

The actin cytoskeleton is well established to be a critical component of the podocyte slit diaphragm (23). Actin organization and stress fibers are regulated through Rho kinase pathways (reviewed in reference 26). To test whether interference of Rho pathways affected barrier function in this model, we used the Rho kinase inhibitors Y27632 and HA 1077. Figure 5B shows a time-dependent increase in flux of >350% with inhibition of Rho kinase by Y-27632. Similar results were seen with HA 1077 (data not shown). Unlike puromycin and PP2, the effects of Rho kinase inhibition on paracellular flux were reversible by 48 h after removal of the inhibitor. Trypan blue staining showed no difference in cell viability in the presence of the inhibitors (5% for both Y27632 and HA1077 *versus* 7% at baseline).

Figure 6 shows the effects on flux of several other signaling modulators and toxins implicated in podocyte pathology. Inhibition of protein kinase C (PKC) with bisindolylmaleimide-1 had no effect, and the G protein modulators aluminum fluoride (G protein activator) and pertussis toxin also had no effect. However, exposure to pertussis toxin for >6 h led to significant increases in cell death. A small but reproducible increase in flux (46%) was seen with the phosphatidylinositol 3-kinase (PI 3-K) inhibitor wortmannin, and angiotensin II (27) also showed a small but significant increase in flux. Cytochalasin D and protamine sulfate (22) demonstrated effects similar to puromycin (Figure 4).

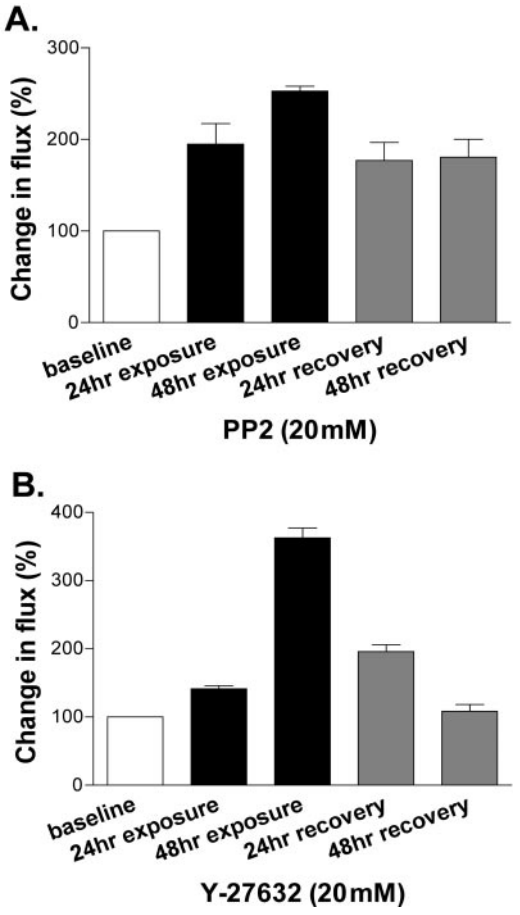


*Figure 5.* Rho and Src inhibition increases flux. (A) Flux rates were determined in the presence of the Src tyrosine kinase inhibitor PP2 (20 $\mu$M). ■, Flux rates after 24 and 48 h of exposure; ▨, flux rates after 48 h of exposure followed by 24 or 48 h of recovery. (B) Flux rates were determined in the presence of the Rho-kinase inhibitor Y-27632 (20 $\mu$M). ■, Flux rate after 24 and 48 h of exposure; ▨, flux rates with 48 h followed by after 24 or 48 h of recovery. All data are with the 70-kD dextran, and all fluxes are relative to baseline (□). Results are the mean of two independent experiments ± SEM with $n = 6$ in each experiment.

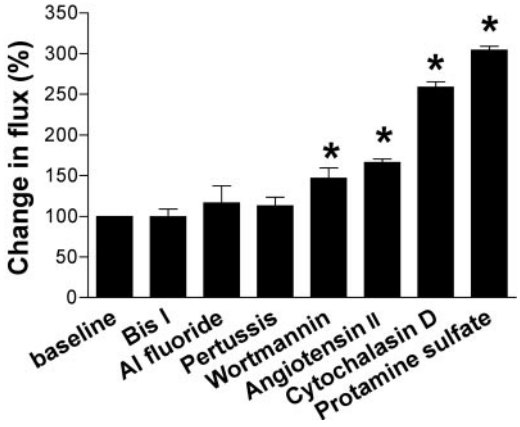


*Figure 6.* Effect of signaling modulators and toxins on flux. Podocytes were incubated with bisindolylmaleimide I (protein kinase C inhibitor) at 200 nM for 48 h, aluminum fluoride (G protein activator) at 2 mM for 48 h, pertussis toxin (G protein inhibitor) at 500 nM for 6 h, wortmannin (phosphatidylinositol 3-kinase inhibitor) at 100 nM for 48 h, angiotensin II at 10 nM for 30 min, cytochalasin D at 400 nM for 30 min, and protamine sulfate at 600 $\mu$g/ml for 8 h. All data are with the 70-kD dextran, and all fluxes are relative to baseline. *Statistically significant increase relative to baseline. Results are the mean of two to four independent experiments ± SEM with $n = 6$ in each experiment.

### *Podocytes Demonstrate Regulated Barrier Assembly in the Calcium Switch Model of Junction Assembly*

One difficult question to answer *in vivo* is how or whether podocyte slit diaphragms can reassemble after injury. The calcium switch is a well-established model used to study assembly of epithelial junctions (18) (Figure 7). In this model, calcium is reduced to micromolar range (LC). This results in intracellular localization of junctional proteins and loss of polarity. Upon "switching" back to NC (millimolar), there is synchronized reassociation of junction proteins within the plasma membrane, reformation of the junctional complex, and reestablishment of cell polarity. No new protein synthesis is required, and this process recapitulates *in vivo* mechanisms (28). We modified the classical calcium switch (18) to determine whether regulated assembly of barrier function occurred in podocytes. Podocytes do not detach from Transwell filters under LC conditions. Exposure of monolayers to Ca/Mg-free HBSS for 90 min (defined as LC) led to a >300% increase in flux (Figure 8A). Figure 8A also shows time-dependent reassembly of the barrier after switching monolayers back to NC medium. There was evidence for partial barrier recovery by 4 to 6 h with further tightening of the barrier over the next 16 to 24 h. By 48 h after the calcium switch, fluxes were indistinguishable from baseline. Cyclohexamide (protein synthesis inhibitor) included during the LC incubation or in both LC and NC switch media had no significant effect on barrier recovery at 24 h (Figure 8B). This finding, in addition to the absence of cell division in differentiated podocytes, suggests that relocalization of pre-existing membrane components is sufficient to account for increased flux in LC and recovery of the barrier by 24 to 48 h.

During junction assembly, several proteins, including ZO-1, develop interactions with the actin cytoskeleton. This can be followed biochemically by monitoring detergent solubility (29). We followed the detergent solubility of four slit diaphragm proteins during the calcium switch: ZO-1, $\alpha$-actinin-4, nephrin, and podocin. Podocin and nephrin did not change solubility characteristics during the calcium switch. Podocin remained nearly 100% soluble, and nephrin was completely detergent resistant (Figure 9A). Both ZO-1 and $\alpha$-actinin showed changes in solubility similar to what has been shown in MDCK cells (30). ZO-1 solubility increased from 35 ± 3% soluble at baseline to 48 ± 1% soluble in LC (Figure 9B). $\alpha$-Actinin-4 solubility increased from 10 ± 3 to 23 ± 2% in LC. After switching to normal calcium, both ZO-1 and $\alpha$-actinin-4 return to baseline solubility by 24 h (Figure 9, B and C).

To address the localization of a junctional protein during the

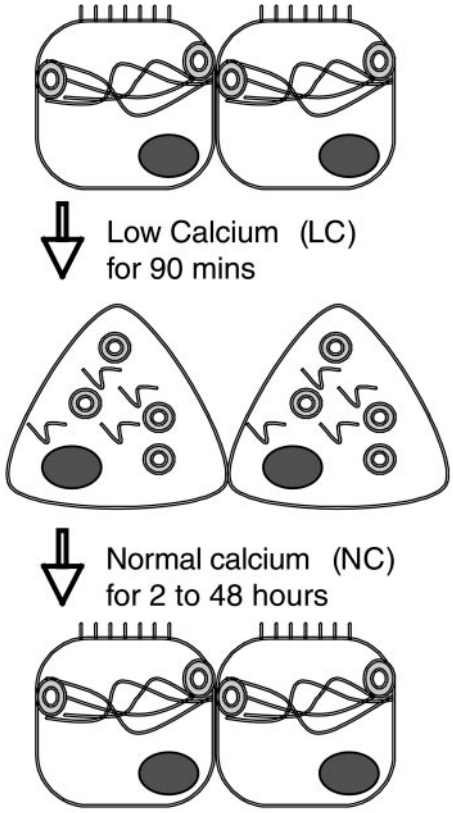


*Figure 7.* Calcium switch model of epithelial junction assembly. Epithelial cells are cultured at confluence and establish an apical-basolateral polarity and "tight" barrier. Changing media to low calcium (LC) results in loss of polarity and internalization of junctional proteins, including ZO-1 and E-cadherin within discrete granules (shown as double circles). ZO-1 becomes less tightly associated with the actin cytoskeleton (wavy lines), and barrier function is lost as a result of junction disruption. Synchronized reassembly of the polarized phenotype and barrier occurs upon switching back to normal calcium (NC) medium. The actin cytoskeleton reassembles, and ZO-1 and other junctional proteins are relocalized into the appropriate membrane domains. The process is not dependent on new protein synthesis.

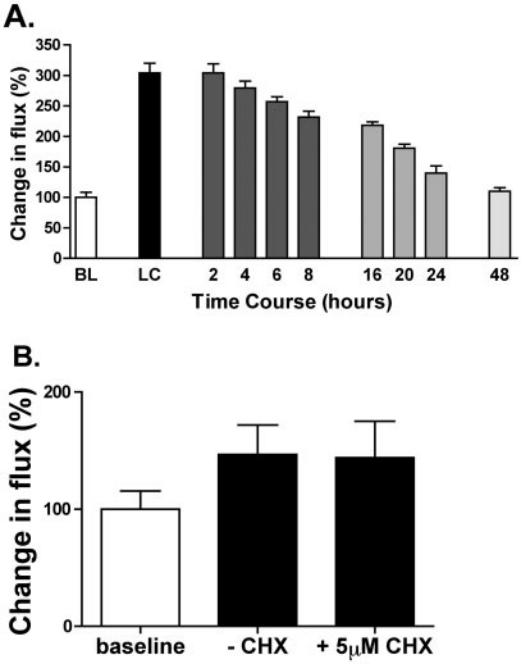


*Figure 8.* Cultured podocytes demonstrate regulated barrier assembly in the calcium switch. (A) Flux rates were measured at baseline and after incubation in Ca/Mg-free Hanks buffered salt solution for 90 min (LC). Flux was measured at specified times after the LC incubation. LC did not lead to significant cellular detachment under these conditions (1.0% in NC, 1.3% in LC). (B) Cyclohexaminde (CHX) inhibits new protein synthesis. −CHX, flux of monolayers at 24 h in NC after calcium switch; +5 $\mu$M CHX, parallel monolayers with CHX in both LC and NC media. All data are with the 70-kD dextran, and all fluxes are relative to baseline (□). Results are the mean of two to six independent experiments ± SEM with $n = 2$ to 4 in each experiment.

calcium switch, we immunolocalized ZO-1 during LC and after switching back to NC medium. At baseline, ZO-1 was seen along the plasma membrane (Figure 10A), whereas exposure for 90 min to LC resulted in internalization and cytoplasmic distribution (Figure 10B). After 4 h in NC, ZO-1 localization remained similar to LC (Figure 10C) and correlated with only a minor increase in barrier function (Figure 8A). Over time, there was slow redistribution of ZO-1 to the plasma membrane that correlated with barrier development. By 24 h in NC, the reassembly was nearly complete with ZO-1 localized at areas of cell–cell contacts (Figure 10E). Phalloidin staining of actin filaments at baseline revealed cortical staining and linear stress fibers, and actin co-localized with ZO-1 at discrete sites of contact between cells (Figure 10A, merge; arrows). In LC, stress fibers have nearly completely disappeared, and there is no co-localization with ZO-1 at any location (Figure 10B, merge). Stress fibers reappear by 4 h in NC and are more highly developed at 16 h in NC. However, the ZO-1 localization remains intracellular, and there is little co-localization with the actin cytoskeleton at these times (Figure 10, C and D, merge). At 24 h in NC, stress fibers are indistinguishable from baseline, and ZO-1 is predominantly relocalized to the plasma membrane. There is punctate co-localization of ZO-1 and actin similar to baseline (Figure 10E, merge; arrows).

## Discussion

The podocyte slit diaphragm is a unique junction with a well-defined set of proteins; however, its regulation and assembly are not completely understood. Using a well-characterized mouse podocyte cell line, we have developed a paracellular permeability (flux) assay that demonstrates (*1*) a differentiation-dependent, size-selective barrier; (*2*) modulation of that barrier by inhibition of specific signal transduction pathways; and (*3*) a calcium-dependent mechanism that leads to reassembly of cell–cell junctions. Using this flux assay in conjunction

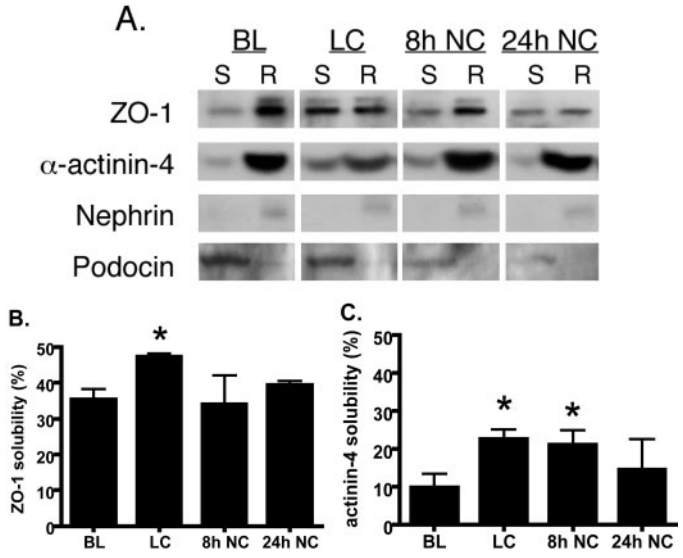


*Figure 9.* Detergent solubility of podocyte proteins during the calcium switch. Differentiated podocytes were grown in 60-mm plastic plates under identical conditions used for flux assays and calcium switch experiments. Detergent-soluble (S) and detergent-resistant (R) fractions were obtained as described in the Materials and Methods section. (A) Analysis by SDS-PAGE and Western blot using specific antibodies. (B) Density of bands was determined and soluble fractions were plotted at each time point as described in the Materials and Methods section. *Statistically significant increase relative to baseline. Results are the mean of three experiments.

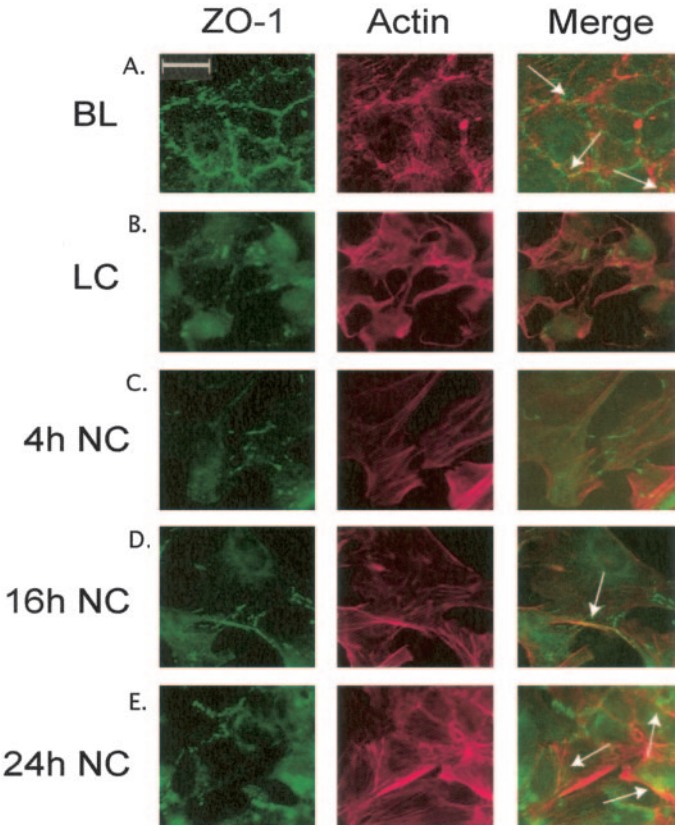


*Figure 10.* ZO-1 and actin reassociate after the calcium switch. Podocytes were differentiated on Transwell filters and subjected to calcium switch as described. At baseline, LC, 4 h of NC, 16 h of NC, and 24 h of NC, filters were excised and stained with phalloidin and ZO-1 as described in the Materials and Methods section. Images were obtained and processed using Spot software as described in the Material and Methods section. Arrows indicate focal areas of co-localization in merged images. Bar = 10 $\mu$M.

with biochemical and immunohistochemical data, we provide evidence for synchronized assembly of barrier function in cultured podocytes.

Size selectivity of the glomerular capillary wall has been recognized for decades. In 1975, Chang *et al.* (3,31) published a landmark description of glomerular permselectivity on the basis of molecular sieving experiments in rats using a micropuncture technique. They showed a 100-fold range in flux over a two- to three-fold range in dextran radius. However, attempts to define which component(s) of the glomerular capillary wall contributes to this selectivity remain inconclusive. Animal studies have produced conflicting results as a result of the inherent inability to separate the contribution of the endothelium, GBM, podocytes, and the tubular epithelium (32,33). Recently, Deen and colleagues (34,35) improved on this approach by stripping cells from the GBM (endothelial and epithelial) and measuring the hydraulic permeability and sieving coefficient of that layer alone. Applying mathematical and biophysical models, the contribution of each component can be inferred but to date cannot be measured directly as has been done with the GBM (36). In fact, mathematical models have attempted to explain permselectivity, but the tools to validate these hypotheses are lacking (37,38). This cultured podocyte cell line provides the first opportunity to define characteristics that are unique to podocytes in the absence of other components, such as the endothelium and GBM. Importantly, this model can be extended to include additional components. We recognize that the barrier function observed in this model is only an approximation to what occurs *in vivo*. Nevertheless, these results suggest that podocytes are sufficient to account for size selectivity and do not require the presence of an intact endothelium and GBM. Furthermore, the absence of a charge effect on barrier properties is consistent with the localization of the charge barrier at the level of the negatively charged glycocalyx in the GBM (4). Taken together, cultured podocytes reveal multiple properties that are useful for studying their role in glomerular selectivity.

Signaling at the slit diaphragm through phosphorylation is well established for nephrin and Neph1, and interactions between the extracellular domains of slit diaphragm proteins are proposed to be important for regulating multiple podocyte functions, including cell survival, transcriptional regulation, polarity signaling, endocytosis, actin remodeling, and mechanosensation (reviewed in reference 16). Nephrin and Neph1 are tyrosine phosphorylated. The Src family nonreceptor tyrosine kinase Fyn binds directly to the cytoplasmic tail of nephrin and mediates nephrin phosphorylation *in vitro* and *in*

*vivo* (25). In addition, targeted deletion of *fyn* in mice resulted in loss of nephrin phosphorylation and foot process effacement with proteinuria (39). Consistent with these observations, inhibition of Src tyrosine signaling with PP2 in cultured podocytes significantly increased flux.

The actin cytoskeleton is central to podocyte structure and function, and podocytes contain a contractile apparatus. There are important connections for actin filaments to the underlying GBM at focal contacts via $\alpha 3\beta 1$ integrins (40), and slit diaphragm proteins are associated with the cortical actin cytoskeleton (23). Our genetic studies have demonstrated that mutations in the actin binding protein $\alpha$-actinin-4 results in familial focal glomerulosclerosis in humans and mice (20,41). Protamine sulfate and cytochalasin D disrupt the actin cytoskeleton and have been shown to effect podocyte foot process dynamics in culture (22), and in this study, both agents significantly increase paracellular flux. Rho pathways are central for actin regulation and stress fiber formation (reviewed in reference 26). Direct evidence for Rho regulation of podocytes and the slit diaphragm is limited, but mice deleted for a Rho regulatory protein develop nephrosis and renal failure (42). One study that examined mechanical stress on this podocyte cell line showed inhibition of radial stress fibers with the Rho kinase inhibitor Y-27632 (43). We show that inhibition of Rho kinase leads to significant and reversible changes in barrier function (Figure 5B). The results suggest that Rho regulation of the actin cytoskeleton is critical to normal podocyte structure and function.

In this model, barrier function was not affected by the G protein modulators aluminum fluoride and pertussis toxin. Aluminum fluoride activates all G protein families, but the absence of an effect on the barrier does not exclude a role for heterotrimeric G proteins in regulating the podocyte barrier. For example, we have shown reciprocal regulation of tight junction assembly in MDCK cells, where the G$\alpha$i family stimulates assembly and G$\alpha$12 inhibits assembly (44–46). Similarly, we found no effect on the barrier with inhibition of PKC. This is in contrast to well-described effects of PKC inhibition on development of tight junctions in MDCK cells (30). Finally, there is evidence that nephrin and CD2AP interact and activate PI 3-K and AKT signaling pathways. Activation of this pathway reduces podocyte apoptosis and may be important for podocyte survival (47). It is interesting that we found that inhibition of PI 3-K with wortmannin and treatment with angiotensin II lead to small increases in flux without affecting cell viability, suggesting additional modulation of the barrier.

The calcium switch process in MDCK cells recapitulates key *in vivo* steps involved in junction assembly (28). Furthermore, there are well-defined interactions of junction proteins with the cytoskeleton and a variety of signaling pathways, including PKC, heterotrimeric G proteins, small G proteins, and tyrosine kinases (48). In podocytes, multiple mechanisms have been described that contribute to foot process effacement, reductions in podocyte numbers through apoptosis, detachment, and reduced proliferation (49). However, direct evidence demonstrating reassembly of the barrier function independent of these other mechanisms is difficult to demonstrate in animal models. We modified the calcium switch model of junction assembly to test whether podocytes can re-establish an intact barrier after LC exposure. We found that there were significant similarities between podocytes and MDCK cells in this model. On the basis of the analogy of the slit diaphragm to a modified adherens junction (7), we predicted that podocytes in culture would demonstrate synchronous assembly of the barrier. Similar to MDCK cells, podocytes showed time-dependent recovery of the barrier that occurred in the absence of new protein synthesis. The time course in podocytes was slower than in MDCK cells, perhaps reflecting the increased complexity of the slit diaphragm. Like MDCK cells, podocytes relocalized ZO-1 from the membrane to intracellular clusters in LC, followed by time-dependent reappearance in the plasma membrane with restoration of normal calcium. In addition, there were reproducible changes in detergent extractability of ZO-1 and $\alpha$-actinin-4, reflecting changes in association with the actin cytoskeleton. Nephrin and podocin did not change solubility characteristics, consistent with their localization in discrete microdomains that are unaffected by LC. The changes in ZO-1 solubility during assembly of the junction is another feature of junction assembly shared with classical epithelial cell junctions. These findings suggest that injured podocytes may be able to re-establish a barrier *in vivo* without initiating new protein synthesis or stimulating potentially detrimental proliferative mechanisms.

In summary, the studies presented here demonstrate the utility of cultured podocytes for investigation into questions of barrier properties and their regulation by specific signal transduction pathways. We demonstrate that cultured podocytes can restore barrier function in a synchronized manner analogous to traditional epithelial cell junctions. These studies provide the foundation for future studies that will define the role of specific signaling pathways in maintaining and assembling the podocyte barrier. These insights then can be applied to *in vivo* models of glomerular disease.

## Acknowledgments

This work was supported by the National Institute of General Medical Sciences Grant GM-5523 and the National Institute of Diabetes and Digestive and Kidney Diseases (NIDDK) Grant DK-65932 (to B.M.D.) and the NIDDK National Research Service Awards DK-62678 (to J.L.H.) and Grant DK-59588 (to M.R.P.).

We graciously acknowledge June Yao, who provided technical assistance with the cultured podocytes and helpful advice throughout the course of this project.

## References

1. Keane WF, Brenner BM, de Zeeuw D, Grunfeld JP, McGill J, Mitch WE, Ribeiro AB, Shahinfar S, Simpson RL, Snapinn SM, Toto R: The risk of developing end-stage renal disease in patients with type 2 diabetes and nephropathy: The RENAAL study. *Kidney Int* 63: 1499–1507, 2003
2. Brenner BM, Hostetter TH, Humes HD: Glomerular permselectivity: Barrier function based on discrimination of molecular size and charge. *Am J Physiol* 234: F455–F460, 1978
3. Chang RS, Robertson CR, Deen WM, Brenner BM: Permselectivity of the glomerular capillary wall to macromolecules. I. Theoretical considerations. *Biophys J* 15: 861–886, 1975

4. Groffen AJ, Veerkamp JH, Monnens LA, van den Heuvel LP: Recent insights into the structure and functions of heparan sulfate proteoglycans in the human glomerular basement membrane. *Nephrol Dial Transplant* 14: 2119–2129, 1999
5. Tryggvason K, Wartiovaara J: Molecular basis of glomerular permselectivity. *Curr Opin Nephrol Hypertens* 10: 543–549, 2001
6. Caulfield JP, Farquhar MG: The permeability of glomerular capillaries to graded dextrans. Identification of the basement membrane as the primary filtration barrier. *J Cell Biol* 63: 883–903, 1974
7. Reiser J, Kriz W, Kretzler M, Mundel P: The glomerular slit diaphragm is a modified adherens junction. *J Am Soc Nephrol* 11: 1–8, 2000
8. Holzman LB, St John PL, Kovari IA, Verma R, Holthofer H, Abrahamson DR: Nephrin localizes to the slit pore of the glomerular epithelial cell. *Kidney Int* 56: 1481–1491, 1999
9. Ruotsalainen V, Ljungberg P, Wartiovaara J, Lenkkeri U, Kestila M, Jalanko H, Holmberg C, Tryggvason K: Nephrin is specifically located at the slit diaphragm of glomerular podocytes. *Proc Natl Acad Sci U S A* 96: 7962–7967, 1999
10. Barletta GM, Kovari IA, Verma RK, Kerjaschki D, Holzman LB: Nephrin and Neph1 co-localize at the podocyte foot process intercellular junction and form cis hetero-oligomers. *J Biol Chem* 278: 19266–19271, 2003
11. Li C, Ruotsalainen V, Tryggvason K, Shaw AS, Miner JH: CD2AP is expressed with nephrin in developing podocytes and is found widely in mature kidney and elsewhere. *Am J Physiol Renal Physiol* 279: F785–F792, 2000
12. Beggs AH, Byers TJ, Knoll JH, Boyce FM, Bruns GA, Kunkel LM: Cloning and characterization of two human skeletal muscle alpha-actinin genes located on chromosomes 1 and 11. *J Biol Chem* 267: 9281–9288, 1992
13. Patrie KM, Drescher AJ, Goyal M, Wiggins RC, Margolis B: The membrane-associated guanylate kinase protein MAGI-1 binds megalin and is present in glomerular podocytes. *J Am Soc Nephrol* 12: 667–677, 2001
14. Kurihara H, Anderson JM, Farquhar MG: Increased Tyr phosphorylation of ZO-1 during modification of tight junctions between glomerular foot processes. *Am J Physiol* 268: F514–F524, 1995
15. Mundel P, Reiser J, Zuniga Mejia Borja A, Pavenstadt H, Davidson GR, Kriz W, Zeller R: Rearrangements of the cytoskeleton and cell contacts induce process formation during differentiation of conditionally immortalized mouse podocyte cell lines. *Exp Cell Res* 236: 248–258, 1997
16. Benzing T: Signaling at the slit diaphragm. *J Am Soc Nephrol* 15: 1382–1391, 2004
17. Mundel P, Reiser J, Kriz W: Induction of differentiation in cultured rat and human podocytes. *J Am Soc Nephrol* 8: 697–705, 1997
18. Gonzalez-Mariscal L, Contreras RG, Bolivar JJ, Ponce A, Chavez De Ramirez B, Cereijido M: Role of calcium in tight junction formation between epithelial cells. *Am J Physiol* 259: C978–C986, 1990
19. Singh AB, Harris RC: Epidermal growth factor receptor activation differentially regulates claudin expression and enhances transepithelial resistance in Madin-Darby canine kidney cells. *J Biol Chem* 279: 3543–3552, 2004
20. Kaplan JM, Kim SH, North KN, Rennke H, Correia LA, Tong HQ, Mathis BJ, Rodriguez-Perez JC, Allen PG, Beggs AH, Pollak MR: Mutations in ACTN4, encoding alpha-actinin-4, cause familial focal segmental glomerulosclerosis. *Nat Genet* 24: 251–256, 2000
21. Ohlson M, Sorensson J, Haraldsson B: A gel-membrane model of glomerular charge and size selectivity in series. *Am J Physiol Renal Physiol* 280: F396–F405, 2001
22. Reiser J, Pixley FJ, Hug A, Kriz W, Smoyer WE, Stanley ER, Mundel P: Regulation of mouse podocyte process dynamics by protein tyrosine phosphatases. *Kidney Int* 57: 2035–2042, 2000
23. Saleem MA, Ni L, Witherden I, Tryggvason K, Ruotsalainen V, Mundel P, Mathieson PW: Co-localization of nephrin, podocin, and the actin cytoskeleton: Evidence for a role in podocyte foot process formation. *Am J Pathol* 161: 1459–1466, 2002
24. Reiser J, Oh J, Shirato I, Asanuma K, Hug A, Mundel TM, Honey K, Ishidoh K, Kominami E, Kreidberg JA, Tomino Y, Mundel P: Podocyte migration during nephrotic syndrome requires a coordinated interplay between cathepsin L and alpha3 integrin. *J Biol Chem* 279: 34827–34832, 2004
25. Verma R, Wharram B, Kovari I, Kunkel R, Nihalani D, Wary KK, Wiggins RC, Killen P, Holzman LB: Fyn binds to and phosphorylates the kidney slit diaphragm component Nephrin. *J Biol Chem* 278: 20716–20723, 2003
26. Etienne-Manneville S, Hall A: Rho GTPases in cell biology. *Nature* 420: 629–635, 2002
27. Gloy J, Henger A, Fischer KG, Nitschke R, Bleich M, Mundel P, Schollmeyer P, Greger R, Pavenstadt H: Angiotensin II modulates cellular functions of podocytes. *Kidney Int Suppl* 67: S168–S170, 1998
28. Rodriguez-Boulan E, Nelson WJ: Morphogenesis of the polarized epithelial cell phenotype. *Science* 245: 718–725, 1989
29. Stuart RO, Sun A, Panichas M, Hebert SC, Brenner BM, Nigam SK: Critical role for intracellular calcium in tight junction biogenesis. *J Cell Physiol* 159: 423–433, 1994
30. Stuart RO, Nigam SK: Regulated assembly of tight junctions by protein kinase C. *Proc Natl Acad Sci U S A* 92: 6072–6076, 1995
31. Chang RL, Ueki IF, Troy JL, Deen WM, Robertson CR, Brenner BM: Permselectivity of the glomerular capillary wall to macromolecules. II. Experimental studies in rats using neutral dextran. *Biophys J* 15: 887–906, 1975
32. Ohlson M, Sorensson J, Haraldsson B: Glomerular size and charge selectivity in the rat as revealed by FITC-ficoll and albumin. *Am J Physiol Renal Physiol* 279: F84–F91, 2000
33. Greive KA, Nikolic-Paterson DJ, Guimaraes MA, Nikolovski J, Pratt LM, Mu W, Atkins RC, Comper WD: Glomerular permselectivity factors are not responsible for the increase in fractional clearance of albumin in rat glomerulonephritis. *Am J Pathol* 159: 1159–1170, 2001
34. Edwards A, Deen WM, Daniels BS: Hindered transport of macromolecules in isolated glomeruli. I. Diffusion across intact and cell-free capillaries. *Biophys J* 72: 204–213, 1997
35. Edwards A, Daniels BS, Deen WM: Hindered transport of macromolecules in isolated glomeruli. II. Convection and pressure effects in basement membrane. *Biophys J* 72: 214–222, 1997
36. Deen WM, Lazzara MJ, Myers BD: Structural determinants of glomerular permeability. *Am J Physiol Renal Physiol* 281: F579–F596, 2001
37. Weinbaum S, Tsay R, Curry FE: A three-dimensional junc-

tion-pore-matrix model for capillary permeability. *Microvasc Res* 44: 85–111, 1992
38. Smithies O: Why the kidney glomerulus does not clog: A gel permeation/diffusion hypothesis of renal function. *Proc Natl Acad Sci U S A* 100: 4108–4113, 2003
39. Yu CC, Yen TS, Lowell CA, DeFranco AL: Lupus-like kidney disease in mice deficient in the Src family tyrosine kinases Lyn and Fyn. *Curr Biol* 11: 34–38, 2001
40. Kreidberg JA, Donovan MJ, Goldstein SL, Rennke H, Shepherd K, Jones RC, Jaenisch R: Alpha 3 beta 1 integrin has a crucial role in kidney and lung organogenesis. *Development* 122: 3537–3547, 1996
41. Yao J, Le TC, Kos CH, Henderson JM, Allen PG, Denker BM, Pollak MR: Alpha-actinin-4-mediated FSGS: An inherited kidney disease caused by an aggregated and rapidly degraded cytoskeletal protein. *PLoS Biol* 2: 787–794, 2004
42. Togawa A, Miyoshi J, Ishizaki H, Tanaka M, Takakura A, Nishioka H, Yoshida H, Doi T, Mizoguchi A, Matsura N, Niho Y, Nishimune Y, Nishikawa S, Takai Y: Progressive impairment of kidneys and reproductive organs in mice lacking Rho GDIalpha. *Oncogene* 18: 5373–5380, 1999
43. Endlich N, Kress KR, Reiser J, Uttenweiler D, Kriz W, Mundel P, Endlich K: Podocytes respond to mechanical stress in vitro. *J Am Soc Nephrol* 12: 413–422, 2001
44. Saha C, Nigam SK, Denker BM: Involvement of Galphai2 in the maintenance and biogenesis of epithelial cell tight junctions. *J Biol Chem* 273: 21629–21633, 1998
45. Meyer TN, Hunt J, Schwesinger C, Denker BM: Galpha12 regulates epithelial cell junctions through Src tyrosine kinases. *Am J Physiol Cell Physiol* 285: C1281–C1293, 2003
46. Meyer TN, Schwesinger C, Denker BM: Zonula occludens-1 is a scaffolding protein for signaling molecules. Galpha(12) directly binds to the Src homology 3 domain and regulates paracellular permeability in epithelial cells. *J Biol Chem* 277: 24855–24858, 2002
47. Huber TB, Hartleben B, Kim J, Schmidts M, Schermer B, Keil A, Egger L, Lecha RL, Borner C, Pavenstadt H, Shaw AS, Walz G, Benzing T: Nephrin and CD2AP associate with phosphoinositide 3-OH kinase and stimulate AKT-dependent signaling. *Mol Cell Biol* 23: 4917–4928, 2003
48. Denker BM, Nigam SK: Molecular structure and assembly of the tight junction. *Am J Physiol* 274: F1–F9, 1998
49. Mundel P, Shankland SJ: Podocyte biology and response to injury. *J Am Soc Nephrol* 13: 3005–3015, 2002